The Astrophysical Journal, 606:542–554, 2004 May 1

A TRANSONIC COLLISIONLESS MODEL OF THE SOLAR WIND

I. Zouganelis,[1] M. Maksimovic,[1] N. Meyer-Vernet,[1] H. Lamy,[2] and K. Issautier[1]

Received 2003 November 6; accepted 2004 January 15

ABSTRACT

Because of the semicollisional nature of the solar wind, the collisionless or exospheric approach and the hydrodynamic one are both inaccurate. However, the advantage of simplicity makes them useful for enlightening us on some basic mechanisms of solar wind acceleration. Previous exospheric models have been able to reproduce winds that were already nearly supersonic at the exobase, the altitude above which there are no collisions. In order to allow transonic solutions, a lower exobase has to be considered, in which case the protons are experiencing a nonmonotonic potential energy profile. This is done in the present work. In this model, the electron velocity distribution in the corona is assumed to be nonthermal. Parametric results are presented and show that the high acceleration obtained does not depend on the details of the nonthermal distributions. This acceleration seems, therefore, to be a robust result produced by the presence of a sufficient number of suprathermal electrons. A method for improving the exospheric description is also given, which consists of mapping particle orbits in terms of their invariants of motion.

Subject headings: acceleration of particles — methods: numerical — solar wind — stars: winds, outflows — Sun: corona

1. INTRODUCTION

Most cosmic bodies eject matter into space, but the solar wind is the first and, up to now, only stellar outflow to have been measured in situ (Neugebauer 1997). Numerous sophisticated models have been developed since Parker's pioneering papers (Parker 1958, 1960) using complicated mechanisms. The different acceleration mechanisms, the origin of the high-speed solar wind, and the associated problem of coronal heating have been recently reviewed in a comprehensive way by Cranmer (2002). However, the solar wind acceleration and its properties are still far from being well understood. The reason for this difficulty is that the solar wind is neither a collision-dominated medium nor a collisionless one. The Knudsen number K_n, which is defined as the ratio of the particle mean free path to the density scale height, is close to unity at Earth's orbit (see, e.g., Hundhausen 1972). This means that neither the hydrodynamic approach nor the purely collisionless one (also called exospheric) are fully appropriate to model the solar wind expansion and to explain its observed properties.

The classical fluid approach is applicable to the extreme regime when $K_n \ll 1$, that is, when the medium is collision-dominated. In this case, the particle velocity distribution functions (VDFs) are Maxwellians, since the medium is assumed to be at local thermodynamic equilibrium. The Euler or Navier-Stokes approximations are applicable and produce a thermally driven wind out of the hot solar corona. There are two problems with this approach: First, the particle VDFs *might* not be Maxwellians at the base of the solar wind. Second, the particle VDFs *are* not Maxwellians in the solar wind. There is an increasing amount of both theoretical (Viñas, Wong, & Klimas 2000; Leubner 2002) and observational evidence (Esser & Edgar 2000) that tends to show that nonthermal VDFs can develop and exist in the high corona and even in the transition region. This is because in a plasma the particle free paths increase rapidly with speed ($\propto v^4$), so that high-energy tails can develop for Knudsen numbers as low as 10^{-3} (Shoub 1983), i.e., even in collisional plasmas. A fortiori, high-energy tails can be expected to be found in the weakly collisional corona and solar wind acceleration region. Indeed, it is well known that the solar wind electron VDFs permanently exhibit nonthermal tails that can be modeled by a halo Maxwellian population (e.g., Feldman et al. 1975) or by the power-law part of a generalized Lorentzian or kappa function (Maksimovic et al. 1997b). In the frame of the fluid approach, which intrinsically cannot handle suprathermal tails, the effect of nonthermal VDFs on the solar wind acceleration can be understood through an increase of the heat flux (Hollweg 1978; Olbert 1981).

An alternative way of taking into account the possible effects of coronal nonthermal distributions is to use a kinetic approach. Among the various kinetic approaches for the solar wind, the simplest one is probably the exospheric one, which totally neglects binary collisions between particles above a given altitude, the "exobase." The first solar wind model of this type was developed by Chamberlain (1960) by analogy with the evaporation of planetary atmospheres. This first exospheric model, modeling the radial expansion of the solar corona from the thermal evaporation of hot coronal protons out of the solar gravitational field, produced a solar breeze. The subsonic speed obtained by the theory was partially due to an inadequate assumption: the electrostatic field was taken so as to ensure hydrostatic equilibrium (Pannekoek 1922; Rosseland 1924), which is inconsistent with an expanding atmosphere. The improved exospheric models by Jensen (1963) and Brandt & Cassinelli (1966) were the first to be able to reproduce supersonic solar wind flows. In these models, multiple exobase locations were assumed, in order to take into account the variable mean free path of the particles as a function of their velocity. However, these models still used the inadequate Pannekoek-Rosseland electric field as an imposed external solution. The actual (outward) ambipolar electric field,

[1] LESIA, Observatoire de Paris, 5 place Jules Janssen, F-92195 Meudon, France; ioannis.zouganelis@obspm.fr.

[2] Belgian Institute for Space Aeronomy, 3 Avenue Circulaire, B-1180 Brussels, Belgium.

which ensures plasma quasi-neutrality and zero electric current, is greater, thereby accelerating protons to greater speeds. Models using this correction (Lemaire & Scherer 1971a; Jockers 1970) produced supersonic winds, but with too small speeds for explaining the fast solar wind ($\sim$700–800 km s^{-1}).

More recently, Maksimovic et al. (1997a) have generalized these calculations by considering non-Maxwellian VDFs for the electrons in the corona, e.g., generalized Lorentzian or kappa functions. With such non-Maxwellian distributions having suprathermal electron tails, a higher electrostatic potential is needed to ensure zero charge and current, therefore producing larger terminal bulk speeds. In essence, this comes about because the electron tail tends to increase the escaping electron flux, so that, to preserve quasi-neutrality, the electrostatic potential increases in order to trap more electrons, which in turn accelerates the protons outward. This model yields a reasonable description of bulk solar wind properties, giving densities, temperatures, and speeds within the ranges observed at 1 AU, even though the details of the VDFs are not reproduced, as expected since collisions are neglected. Its major interest is the prediction of high speeds without assuming extremely large coronal temperatures and/or additional heating of the outer corona, as is needed in hydrodynamic models. More basically, the main achievement of exospheric models is to furnish a possible driving mechanism for the fast solar wind, with a single assumption: the suprathermal electron VDF at the exobase.

However, the Maksimovic et al. (1997a) model cannot be applied for low-altitude exobases, which is the case of coronal holes, from where emanates the fast solar wind. In these deep coronal layers, the gravitational force acting on the protons is stronger than the electric one, so that the total potential for the protons is attractive out to some distance where the two forces balance each other. Farther out, the outward electric force dominates. This means that the total potential energy for the protons is not monotonic, presenting a maximum at a certain distance from the exobase (Jockers 1970), and therefore not all the protons present at the exobase are able to escape. The presence of such a maximum is not taken into account in the Maksimovic et al. (1997a) model or in the Lemaire & Scherer (1971a) one, since both models started beyond the vicinity of the sonic point.

The purpose of the present paper is to study the effect of nonthermal electron VDFs in the frame of a transonic exospheric solar wind model. We use a special technique described by Jockers (1970) and Khazanov et al. (1998) consisting of mapping particle orbits in terms of the invariants of motion. The same problem has been recently considered by Lamy et al. (2003) using a different formulation, which involves an approximation relative to the escaping-particle rate (see Appendix). The present work, which uses the same approximation, sets the basis of an exact exospheric description of the solar wind acceleration. The reader should, however, have in mind that the present model is still a very simplified one that does not pretend to describe all solar wind properties. Instead, it may be useful to determine some basic aspects and a possible driving mechanism of the solar wind, avoiding ad hoc assumptions on energy dissipation and using as few free parameters as possible.

In § 2 we recall the basics of an exospheric solar wind model. In § 3 we outline the difficulties that arise when dealing with a nonmonotonic potential energy for the protons and describe the technique used to calculate the interplanetary electrostatic potential. In § 4 we deal with non-Maxwellian electron distribution functions and consider three cases: a kappa distribution, a sum of two Maxwellian distributions (a core and a halo), and a sum of a Maxwellian and a kappa. The latter distribution is rather general and reproduces the main features of VDFs observed in space plasmas: a Maxwellian profile at low speeds and a high-energy tail with a power-law shape. In § 5 we describe the results of our model and compare them with observations. A summary and final remarks are given in § 6.

2. BASICS OF A KINETIC COLLISIONLESS MODEL

In exospheric or kinetic collisionless models, a specific altitude, called the exobase, is defined as an abrupt boundary between the collision-dominated region (in which a hydrodynamic approach is valid) and a completely collisionless one. This boundary is usually defined as the distance r_0 from the center of the Sun where the Knudsen number K_n is equal to unity, i.e., where the Coulomb mean free path becomes equal to the local density scale height. Although the mean free path depends on the particle temperature, and therefore the exobase should be different for protons and electrons, a common exobase is assumed in order to simplify the calculations. Furthermore, in order to concentrate on the basic physics and since the exobase location is defined from parameters that are not accurately known, we put the exobase at the surface of the Sun; i.e., $r_0 = 1\ R_\odot$. This stands as an approximation of a more realistic value that should be slightly greater, and has no important qualitative impact on the results.

The collisionless nature of the plasma above the exobase allows one to calculate the velocity distribution of each particle species as a function of the distribution at the exobase by using Liouville's theorem with conservation of energy E and magnetic moment μ in order to solve the Vlasov equation for a time-stationary wind. These two constants of motion are defined as

$$E = \frac{mv^2}{2} + m\phi_g + Ze\,\phi_E, \tag{1}$$

$$\mu = \frac{mv_\perp^2}{2B}, \tag{2}$$

where v is the speed of the particle of mass m, Ze is its charge, $\phi_g(r) = -M_\odot G/r$ is the gravitational potential, $\phi_E(r)$ is the interplanetary electrostatic potential, and $v_\perp$ is the velocity component perpendicular to the magnetic field vector $\boldsymbol{B}$. The choice of using the constants of motion (E, μ) instead of the speed and pitch angle is convenient since it removes the spatial dependence in the distribution function. In a purely collisionless model, the magnetic moment is conserved, even though this may not be true for protons in the high-speed wind (Schwartz & Marsch 1983).

The classification of particles in different species is based on their trajectories along magnetic field lines. These trajectories depend on the velocity and pitch angle at the exobase or, correspondingly, on their energy and magnetic moment. There are four different classes of trajectories: incoming, escaping, ballistic, and trapped particles, as defined in Lemaire & Scherer (1971a). Escaping particles are the ones that have enough energy to escape from the Sun, while ballistic ones are those with insufficient energy that are returning toward it. Other nonescaping particles are the trapped ones, which do not have enough energy to escape but whose inclination to the magnetic field lines is large enough that they are reflected by the magnetic

mirror force before reaching the exobase r_0. Finally, there are particles coming from infinity, called "incoming" ones, which are neglected. Indeed, because of the postulated absence of collisions above the exobase, no particles, in principle, are backscattered in the downward loss cone. This assumption can be relaxed in future applications of our model, but it is not unreasonable in the fully collisionless case.

Once a VDF f_0 is assumed at the exobase level r_0, the VDF f at any larger distance r is uniquely determined by Liouville's theorem. The electron and proton distributions f_e and f_p and their moments—in particular, the electron and proton densities n_e and n_p—are functions of the electric potential $\phi_E(r)$. The quasi-neutrality condition $n_e(r) = n_p(r)$ is then used to determine, by an iterative method, the value of the potential ϕ_E at any altitude r. The iterative process is stopped when the estimation of $\phi_E(r)$ is adequate within the required precision. In addition, we impose the equality of the electron and proton fluxes at the exobase, in order to ensure a zero electric current. (Note that the current will also be zero everywhere because fluxes of both kinds of particles vary as r^{-2}). Then it is possible to calculate the other moments, e.g., pressures and heat flux, at any distance r. Strictly speaking, one should solve Poisson's equation instead of imposing quasi-neutrality. However, for scales much greater than the Debye length, which is the case here, the quasi-neutrality condition provides a very good approximation of the electrostatic potential distribution in the solar wind.

Another assumption is the use of a radial interplanetary magnetic field $B(r)$, varying as r^{-2}, which means that the rotation of the Sun, as well as a possible superradial expansion of the wind, are neglected. As was shown by Chen et al. (1972) with a fluid approach and more recently by Pierrard et al. (2001) with an exospheric approach using kappa distributions, a spiral magnetic field does not change significantly the wind density and bulk speed. However, temperatures are modified, especially their anisotropies. In any case, the magnetic field is not very far from radial up to about 1 AU, so this approximation is reasonable in the framework of the present model, in which we study fundamental aspects of the fast solar wind coming from coronal holes, i.e., at rather high heliolatitudes. Nevertheless, a superradial expansion of the wind is an ingredient that might influence the results, but it is neglected in this zero-order approximation in order to avoid additional free parameters.

3. NONMONOTONIC PROTON POTENTIAL ENERGY

Solar wind protons are subjected to the attractive gravitational potential $\phi_g(r)$ of the Sun and to the repulsive interplanetary electrostatic field $\phi_E(r)$. Their total potential energy is thus $\Psi(r) = m\phi_g(r) + e\phi_E(r)$, which reaches a maximum at some radial distance $r_{\max}$. Such a maximum occurs because the electric force is expected to decrease slower than r^{-2}, so that this force, which pushes the protons outward, should dominate gravity at large distances (Jockers 1970; Meyer-Vernet et al. 2003). Below this altitude $r_{\max}$, the gravitational force is larger than the electrostatic one and the total potential is attractive. The opposite is true above $r_{\max}$, forcing all the protons present at these altitudes to escape.

Until now, exospheric models using suprathermal distributions for the electrons have considered a monotonic potential profile for the protons. This means that the exobase was located above the maximum, i.e., at $r_0 > r_{\max}$, so that the wind was already supersonic at the exobase level. All protons were escaping, since they were experiencing a monotonic repulsive total potential. Even though these models gave supersonic solutions, they were incomplete because they did not consider the transition from subsonic to supersonic speeds. Note that in the general case the Parker's critical point does not coincide with the potential maximum $r_{\max}$ and is generally below it (Meyer-Vernet et al. 2003), even though these two points are relatively close to each other. This is also true in recent kinetic simulations taking into account Coulombian collisions (Landi & Pantellini 2003). In the special case of an increasing temperature with $T \propto r^{3/4}$, these two points coincide (Scudder 1996).

For coronal holes, from where emanates the fast solar wind, the relation $r_0 > r_{\max}$ is no longer valid. Indeed, in that case, the exobase is located deeper in the corona, because of the lower density of coronal holes. At these altitudes, some protons cannot escape from the gravitational well of the Sun and become ballistic or trapped. Such a case has been considered by Jockers (1970), who, however, did not consider nonthermal distributions for the electrons. Recently, Liemohn & Khazanov (1998) have given a more general theoretical framework for dealing with arbitrary potential profiles, while Khazanov et al. (1998) have applied it to describe the precipitation of a magnetospherically trapped hot population and the outflow from the high-latitude ionosphere.

With a nonmonotonic potential, the validity of previous exospheric models is questionable because of the violation of constraints given by Chiu & Schulz (1978) regarding the first and second derivatives of the electrostatic potential with respect to the magnetic field. The technique described by Liemohn & Khazanov (1998) consists of mapping particle orbits in terms of the invariants of motion. This technique has the interest of removing the spatial dependence of the distributions, which can now be written as $f(E, \mu)$. The density, flux, and pressures are then given by the following expressions:

$$n = \frac{\sqrt{2}\pi B}{m^{3/2}} \int \frac{f(E,\mu)}{\sqrt{E - \mu B - \Psi}} dE\, d\mu, \tag{3}$$

$$F = \frac{2\pi B}{m^2} \int f(E,\mu) dE\, d\mu, \tag{4}$$

$$P_{\parallel} = \left(\frac{2}{m}\right)^{3/2} \pi B \int \sqrt{E - \mu B - \Psi} f(E,\mu) dE\, d\mu, \tag{5}$$

$$P_{\perp} = \frac{\sqrt{2}\pi B^2}{m^{3/2}} \int \frac{\mu f(E,\mu)}{\sqrt{E - \mu B - \Psi}} dE\, d\mu. \tag{6}$$

The spatial dependence is now transferred into the region of integration (over which the moments are calculated) in E-μ space. The basic problem is the accessibility of the different particle populations in this space. This technique has been recently outlined by Zouganelis et al. (2003); for a full detailed description of the method, we refer the reader to the paper by Liemohn & Khazanov (1998). In the Appendix, we describe some elementary concepts of this technique, as applied to the solar wind.

4. NONTHERMAL ELECTRON DISTRIBUTIONS

Maxwellian distributions can be used for the solar wind protons, but solar wind electrons permanently exhibit significant suprathermal tails in their distribution functions. The fundamental reason for the electrons to be non-Maxwellian is

that fast electrons collide much less frequently than slow ones because of their greater free path, so that they cannot relax to a Maxwellian. Usually, the solar wind electron distributions are fitted to a sum of two Maxwellians: a core of cold electrons and a halo of hot ones (see for instance Feldman et al. 1975; Pilipp et al. 1987). An alternative to the core/halo model has been proposed by Vasyliunas (1968), a generalized Lorentzian or kappa function, which has been introduced by Scudder (1992) to explain high coronal temperatures by velocity filtration. An interesting combination of these two distributions is the sum of a cold Maxwellian and a hot kappa as a halo component. The sum of two Maxwellians is then a particular case of this last one.

4.1. *Kappa Function*

The electron distributions in the solar wind are observed to have important high-velocity tails, and a convenient way to fit them is to use kappa (or generalized Lorentzian) functions. This was done by Maksimovic et al. (1997b) using *Ulysses* data. Some recent observations (Lin et al. 1997) suggest the existence of a superhalo-Maxwellian population that does not seem to be fitted by a kappa function. However, this part of the distribution ($v \gg v_{\rm th}$) does not contribute in our model. The main interest of kappa distributions is that they require one fewer parameter than the core/halo model, and in addition they have a power-law suprathermal tail, as is often observed in space (Vasyliunas 1968). Recently, there have been some attempts to find a physical explanation of these distributions (Collier 1993; Ma & Summers 1999; Treumann 1999; Leubner 2002) and to study how nonthermal electron tails can be generated in the lower chromosphere (Viñas et al. 2000) and the corona (Vocks & Mann 2003).

Maksimovic et al. (1997a) have considered for the first time kappa distributions in a kinetic collisionless model of the solar wind, but with the restriction of a monotonic potential energy for the protons, thus resulting in a wind that is already supersonic at the exobase. The kappa function is defined as

$$f_\kappa(\boldsymbol{v}) = \frac{n_{e0}}{(\pi\kappa v_\kappa^2)^{3/2}} \frac{\Gamma(\kappa+1)}{\Gamma(\kappa-1/2)} \left(1+\frac{v^2}{\kappa v_\kappa^2}\right)^{-(\kappa+1)}, \quad (7)$$

where $\Gamma(x)$ is the Gamma function and v_κ is the thermal speed defined by

$$v_\kappa = \left(\frac{2\kappa-3}{\kappa}\frac{k_{\rm B}T_e}{m_e}\right)^{1/2}, \quad (8)$$

where $k_{\rm B}$ is the Boltzmann constant and m_e is the electron mass.

For speeds v smaller or comparable to v_κ, the kappa distribution, for any value $\kappa \geq 2.5$, is rather close to a Maxwellian having the same thermal speed. However, the equivalent kappa temperature T_κ (defined from the second moment of the VDF as the ratio between pressure and density) is related to the Maxwellian one $T_{\rm M}$ by $T_\kappa = [\kappa/(\kappa-3/2)]T_{\rm M}$. For $v \gg v_\kappa$, the kappa distribution decreases with v as a power law ($f_\kappa \propto v^{-2(\kappa+1)}$). In the limit $\kappa \to \infty$, $f_\kappa(v)$ reduces to a Maxwellian distribution with $T_{\kappa\to\infty} = T_{\rm M}$. Note that when electron distributions measured in the solar wind are fitted with kappa functions, the parameter κ_e for the electrons ranges from 2 to 5 (Maksimovic et al. 1997b).

The basic equations for an exospheric model with kappa distributions are given by Pierrard & Lemaire (1996). Those concerning the electrons are still valid in our model since the potential energy of electrons is an increasing function of the distance. When considering a kappa VDF, we therefore use equations (5)–(34) by Pierrard & Lemaire (1996), which give the density, flux, pressure, and energy flux of the electrons above the exobase; these quantities correspond respectively to the zero-, first-, second-, and third-order moments of the kappa VDF.

4.2. *A Sum of Two Maxwellians*

The kappa VDF is the most convenient function modeling distributions with high-energy tails. However, there are several reasons for considering other kinds of nonthermal VDFs. First, there is currently no agreed-upon physical explanation for kappa VDFs and, even though they are rather close to a Maxwellian at low velocities, they may not be as close to it as observed. Second, moments of order higher than $2\kappa - 1$ diverge, since $f_\kappa \propto v^{-2\kappa-2}$ at large speeds. Note however that this is merely a mathematical difficulty that has no impact on our model since it does not involve these higher order moments. Third, from Liouville's theorem, the value of κ, which represents the nonthermal character, remains constant with altitude in the absence of collisions. Actually, one should expect that as distance increases and there are fewer collisions, the electron VDFs should present stronger suprathermal tails, so that κ should decrease with distance. Indeed, recent observations in the corona suggest distributions having a nonthermal character that increases with altitude (Esser & Edgar 2000).

For these reasons we also consider a sum of two Maxwellians, which is the classical way of representing electron VDFs in the solar wind (Feldman et al. 1975; Pilipp et al. 1987). Such a VDF does not have any of the above-mentioned disadvantages. If n_{c0} and T_{c0} are respectively the electron density and temperature at the exobase for the cold (core) component and n_{h0} and T_{h0} are the same quantities for the hot (halo) component, we can define their relative importance by two parameters: $\alpha_0 = n_{h0}/n_{c0}$ and $\tau_0 = T_{h0}/T_{c0}$. The total density and temperature at the exobase is then given by $n_0 = n_{c0}(1+\alpha_0)$ and $T_{e0} = [(1+\alpha_0\tau_0)/(1+\alpha_0)]T_{c0}$. At any altitude the density is just the sum of the two densities, the core and the halo one. The same is true for the fluxes and pressures. What is interesting is that now the parameters α and τ are functions of the distance, so that the nonthermal nature of the distribution is not held constant contrary to the case of a kappa distribution. Note that in this purely collisionless model the core and halo components do not interact with one another (as in, e.g., the hydrodynamic core-halo model of Chen, Esser, & Hu 2003). The density, flux, and pressures are defined as the moments of the distribution function for each particle population (escaping, ballistic, and trapped), as given in Pierrard & Lemaire (1996). Analytical expressions of these quantities can be calculated as a function of the electrostatic potential $\phi_E(r)$. For a Maxwellian VDF, they are similar to those given in Lemaire & Scherer (1971b) and will not be expressed here. These expressions are to be used for both the core and the halo components.

4.3. *A Sum of a Maxwellian and a Kappa Function*

A more general form for the distribution function is the sum of a Maxwellian core and a kappa halo. This function is closer to a Maxwellian at low speeds than a kappa distribution and

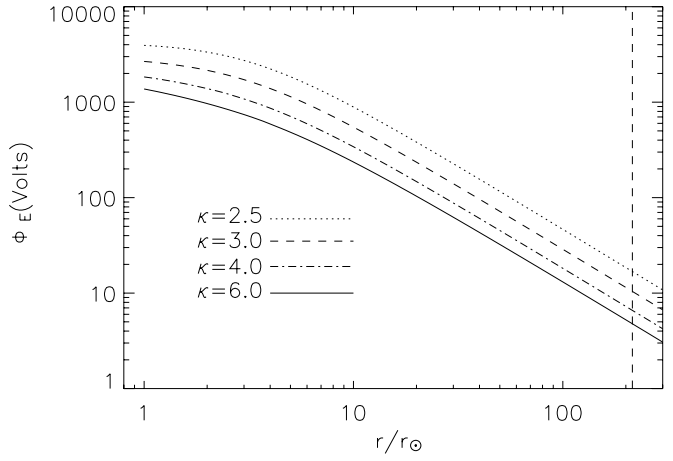

FIG. 1.—Interplanetary electrostatic potential for $\kappa = 2.5$, 3.0, 4.0, and 6.0. The dashed vertical line indicates Earth's orbit.

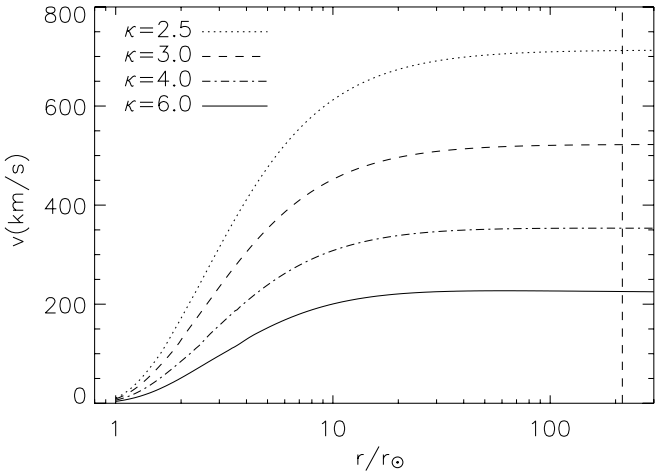

FIG. 3.—Bulk speed profiles for $\kappa = 2.5$, 3.0, 4.0, and 6.0. The dashed vertical line indicates Earth's orbit.

has the advantage that the nonthermal character is not held constant, as was the case with a kappa VDF. We use the same definitions of α_0 and τ_0 as before. Note that for $\kappa \to \infty$ the VDF reduces to a sum of two Maxwellians. The expressions of the moments used are those for a Maxwellian for the core and equations (5)–(34) by Pierrard & Lemaire (1996) for the kappa halo.

5. RESULTS AND DISCUSSION

As explained in § 2, the exobase location is approximated to be at $r_0 = 1\ R_\odot$ with no serious impact on the results. We assume for the temperatures at the exobase $T_{e0} = 10^6$ K and $T_{p0} = 2T_{e0}$, in the range of values observed in coronal holes (Cranmer 2002). The density at the exobase does not affect the results of velocity or temperature and is just a multiplicative factor in the density profiles.

Let us first consider a kappa VDF for the electrons as described in § 4.1. The calculated electric potential and the total potential energy of the protons are plotted in Figures 1 and 2, respectively, for different values of κ ranging from $\kappa = 6$ to $\kappa = 2.5$, a case with a conspicuous suprathermal tail. Note that we use $\kappa > 2$ in order for the energy flux to be finite. One sees that the value of the maximum of potential increases and its distance $r_{\max}$ decreases as κ decreases. This is because with more suprathermal electrons, a stronger electric potential is needed to preserve quasi-neutrality. For a Maxwellian VDF ($\kappa \to \infty$), the total proton potential energy increases monotonically and tends asymptotically to zero (remaining always negative).

The bulk speed—the ratio between flux and density—is shown in Figure 3 for a kappa distribution. A high terminal bulk speed (>700 km s^{-1}) is obtained when the suprathermal tail is conspicuous ($\kappa = 2.5$). This is due to the large value of the maximum in ion potential energy ($\approx 14 k_B T_{p0}$), which is transformed into kinetic energy of the escaping protons as they are accelerated above $r_{\max}$. An important remark is that the major part of this high terminal bulk speed is obtained within a small heliocentric distance ($\approx 10\ R_\odot$); this is due to the large acceleration represented by the large slope of the potential above $r_{\max}$. Note that this is the largest terminal bulk speed obtained by this model with a kappa VDF.

The density profiles are shown in Figure 4. One sees that they are nearly independent of the value of κ. The density at 1 AU depends on the one taken at the exobase. In this figure we assumed an exobase density $n_0 = 1.8 \times 10^{13}$ m^{-3}, which corresponds to the density of a coronal hole extrapolated to $r_0 = 1\ R_\odot$ as given by Koutchmy (1977) in line with recent

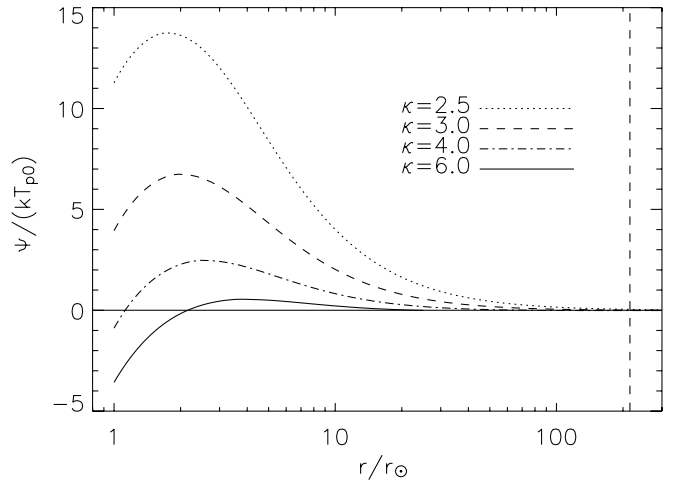

FIG. 2.—Total proton potential energy for $\kappa = 2.5$, 3.0, 4.0, and 6.0. The dashed vertical line indicates Earth's orbit. The energy is normalized to $k_B T_{p0}$.

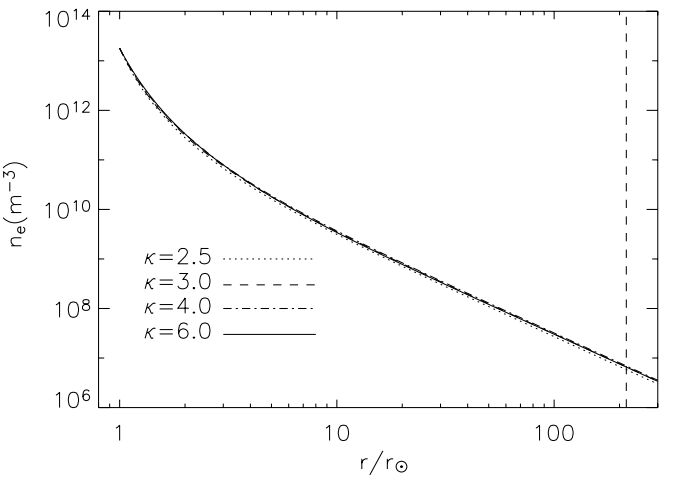

FIG. 4.—Electron density profiles for $\kappa = 2.5$, 3.0, 4.0, and 6.0. The dashed vertical line indicates Earth's orbit.

studies on atmospheric and coronal electron densities (Esser & Sasselov 1999). With this density, the model yields a density of about 6 cm^{-3} at 1 AU, of the same order as observed in situ. Note that the rest of the results do not depend on the density.

This analysis bears out previous results of an exospheric model using kappa VDFs (Maksimovic et al. 1997a). There are however two basic differences. In the present work the velocity profiles span the entire domain from the subsonic to the supersonic regime, which was not the case when the exobase was located above r_{max}. The second difference is that we obtain high bulk speeds with more reasonable temperatures at the exobase. Note however that a direct comparison cannot be done because of a slightly different exobase definition resulting in different proton temperatures at the exobase. In any case, both models can produce high bulk speeds without assuming an additional (ad hoc) heating mechanism in the outer corona, as is generally postulated in hydrodynamic models. Furthermore, the fact that a faster wind is obtained with low values of κ agrees with observations showing that VDFs have large suprathermal tails in the fast solar wind but are closer to a Maxwellian in the slow wind (Maksimovic et al. 1997b).

The large suprathermal tails for low values of κ have another important consequence. They make the electron temperatures increase considerably with distance up to a maximum ($\approx 7 \times 10^6$ K) within a few solar radii. This maximum in electron temperature is smaller for larger values of κ and disappears as $\kappa \rightarrow \infty$ (Fig. 5), as does the maximum in the total potential energy of protons. This temperature increase is a direct consequence of filtration of the non-Maxwellian VDF by the attracting electrostatic potential (Scudder 1992). This large temperature increase is not observed, which suggests that kappa functions may not be adequate to model VDFs having suprathermal tails in the corona.

Let us now consider the results obtained with electron distributions made of a sum of two Maxwellians or a sum of a Maxwellian core and a kappa halo. On the whole the results are rather similar. For the same acceleration we obtain approximately the same temperature increase as in the kappa case, as we see in Figure 6 ($\alpha_0 = 0.03$, $\tau_0 = 5$, and $\kappa = 2.5$), which corresponds to a terminal bulk speed of $\sim$770 km s^{-1}. We deduce that the temperature increase is not an artifact of kappa VDFs, but a general behavior of nonthermal distributions. For a given terminal bulk speed the filtration mechanism results in the same temperature increase. It is important to note that collisionless models are expected to give correct electron temperatures (Meyer-Vernet & Issautier 1998), because collisions with other particles do not significantly affect the electron energy, whereas collisions between electrons do not change their total temperature. In any case we should remind the reader that the present model is still a zero-order one that is intended to explore the basic physics of the wind acceleration but should not be expected to reproduce all observations in a detailed way, because it involves very few free parameters.

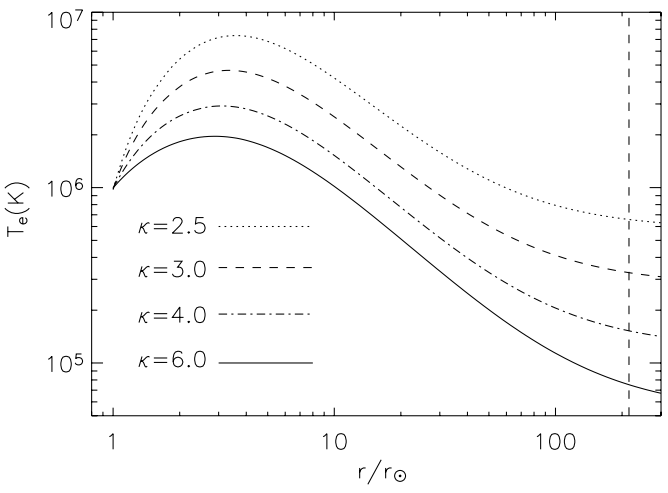

FIG. 5.—Electron temperature profiles for $\kappa = 2.5$, 3.0, 4.0, and 6.0. The dashed vertical line indicates Earth's orbit.

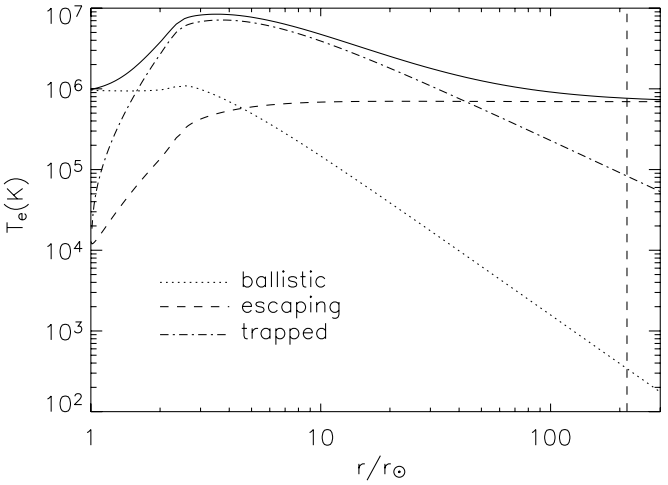

FIG. 6.—Electron temperature profile (*solid line*) for a sum of a Maxwellian core and a kappa halo with $\alpha = 0.03$, $\tau = 5$, and $\kappa = 2.5$. The other lines show the contributions of the different particle species. The dashed vertical line indicates Earth's orbit.

Figure 6 shows also the contributions of the different particle species to the total electron temperature. At large distances the temperature profile is the sum of a term $\propto r^{-4/3}$ plus a constant. The $r^{-4/3}$ term comes from the isotropically distributed electrons (ballistic and trapped) confined by the heliospheric electric potential, which is found to have the same radial variation at large distances. The constant term comes from the parallel temperature of the escaping electrons. This agrees with analytical results by Meyer-Vernet & Issautier (1998) that do not depend on the VDFs in the corona but were obtained with a monotonic proton potential profile. When the proton potential energy is nonmonotonic, the asymptotic electron temperature profile is still the sum of a term varying as $r^{-4/3}$ plus a constant (Meyer-Vernet et al. 2003), but the relative importance of these terms is not necessarily the same.

In Figure 7 we show results for a sum of two Maxwellians. The diagram shows contours of the terminal bulk speed (at 1 AU) as function of α_0 and τ_0, where we can see that this kind of VDF is able to explain the values of the fast wind speed (700–800 km s^{-1}). The terminal bulk speed increases with increasing τ_0, which is not surprising since the halo temperature increases. Concerning the parameter α_0, the terminal bulk speed behaves differently. One sees that the terminal speed has a maximum for some value of α_0 (for a given τ_0). This is reasonable since for $\alpha_0 \rightarrow 0$ and $\alpha_0 \rightarrow \infty$ we have just one Maxwellian with temperature T_{e0}, and for all values of α_0 between these limits, the electron VDF is nonthermal, giving rise to a more important acceleration because of the velocity filtration mechanism. In addition, close to these limits

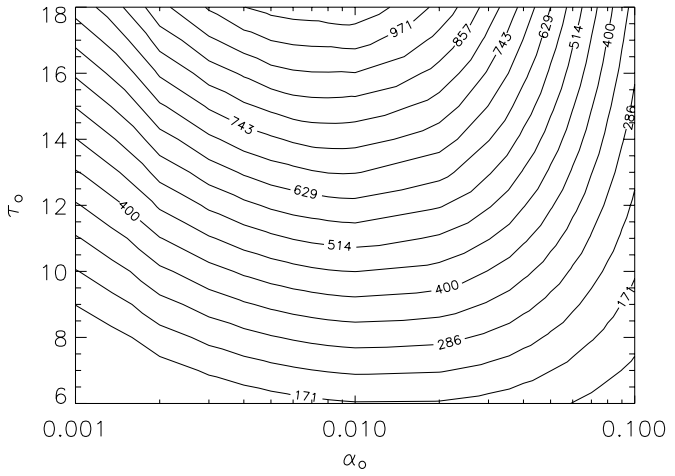

FIG. 7.—Contours of the terminal bulk speed (at 1 AU) in kilometers per second for a sum of two Maxwellians for the electrons as a function of α_0 and τ_0 at the exobase.

the terminal bulk speed becomes independent of τ_0, since there is just only one VDF. That makes the contour lines vertical.

When using a sum of a Maxwellian core and a kappa halo (for instance, with $\kappa = 2.5$), the contour plot of the terminal bulk speed is quite similar to the previous one, as shown in Figure 8. The main difference is the higher acceleration, which is due to the use of the kappa function. The maxima for a given τ_0 are now displaced to the right (to larger values of α_0). This is because for $\alpha_0 \rightarrow \infty$, the VDF is now just a single kappa accelerating the wind more than a single Maxwellian. It is important to note that we can obtain very high wind speeds even without using a kappa VDF (Fig. 7). This shows that the acceleration is not just a consequence of the kappa function, but results from nonthermal distributions, as expected. There are no restrictions on α_0 and τ_0 (as in the case of the kappa VDF, where we have to take $\kappa > 2$), but one should constrain these parameters by coronal observations or by future in situ measurements close to the Sun.

6. SUMMARY AND FINAL REMARKS

In the present work we have described a collisionless model of the solar wind acceleration assuming nonthermal velocity distribution functions in the corona. The base altitude of the fast wind was taken to be low enough (case of coronal holes) to consider the transition from the subsonic to the supersonic regime. This required a special resolution method considering a nonmonotonic potential energy of the protons. An approximation regarding the escaping-particle rate has been used (see Appendix) in order to obtain the electrostatic potential in a self-consistent way.

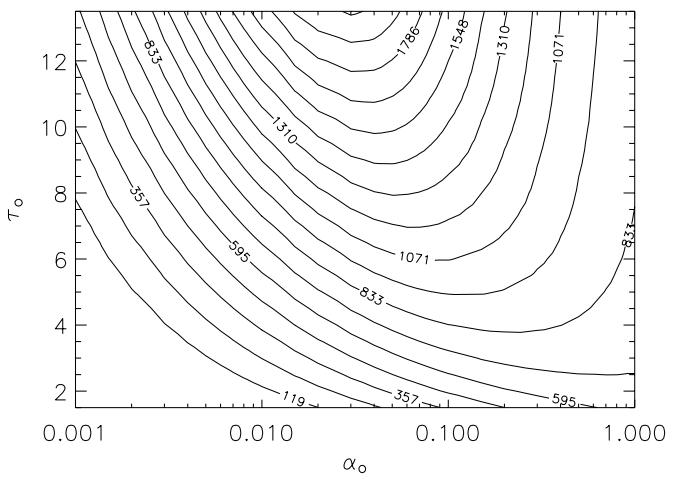

FIG. 8.—As in Fig. 7, but for a sum of a Maxwellian core and a kappa halo with $\kappa = 2.5$.

There are two important results in our work: First, we have shown the fundamental role of nonthermal electron velocity distributions in accelerating the wind. The high value of the terminal bulk speed is not just an artifact of the use of kappa functions. Such speeds can be obtained also with a sum of two Maxwellians (a cold and a hot one), which is the most commonly used model to represent the observed electron distributions.

Second, there is a more important acceleration of the wind, compared with previous exospheric models. This is due to the nonmonotonic proton potential profile that forces some of the protons to return back to the Sun and therefore reduces the escaping proton flux. As a consequence, the interplanetary electrostatic potential accelerating the wind is enhanced. It is also important to note that the terminal bulk speed is anticorrelated with the ratio of proton to electron temperatures at the base of the wind and that therefore there is no need to assume large coronal temperatures or additional heating of the outer region of the corona in order to explain fast wind speeds.

An inherent property of nonthermal distributions is the velocity filtration mechanism (Scudder 1992). This results in an increase of the electron temperature within a few solar radii. One problem of the present model is the relatively high maximum reached by the electron temperature when using highly nonthermal electron distributions at the exobase to produce the fast wind. This problem could be due to the approximation used in order to obtain the potential in a self-consistent way. A full treatment of the problem with no approximation would increase the terminal bulk speed, but the influence on the electron temperature is not known a priori. Another ingredient that might influence the results is a possible superradial expansion of the wind.

An apparent inconsistency of our model is the population of trapped electrons. Trapped electrons can only be produced if collisions decelerate ballistic electrons in order to be reflected before reaching the exobase. Strictly speaking, in the present fully collisionless model, trapped electron orbits should not be populated. If so, however, the VDF would have a strong discontinuity that should be rapidly smoothed out by even a very small level of collisions. Hence, we think that it is more reasonable to set this population at a level ensuring that the VDF has no discontinuity for nonescaping particles, as was done in all previous exospheric models.

The collisionless nature of our model is an inherent drawback. Recent kinetic simulations of the solar wind taking into account binary collisions between particles (Landi & Pantellini 2003) suggest that collisions might be an important ingredient for accelerating the wind to supersonic speeds, but this latter work does not consider nonthermal electron distributions. The role of collisions has also been studied by Landi & Pantellini (2001) and Dorelli & Scudder (2003) for the solar corona. The electron heat flux, which plays a key role in the solar wind acceleration, seems to be essentially determined by the collisionless high-energy tail. This suggests that even though the present model neglects collisions, it may correctly describe a large part of the physics involved in the

effect of nonthermal electron distributions. In order to better explain the observational properties, additional physical ingredients should be taken into account, which will be the purpose of a future study.

We are grateful to A. Mangeney, M. Moncuquet, and F. Pantellini for stimulating discussions and useful comments on the manuscript. We also thank the anonymous referee for helpful suggestions that improved this paper.

APPENDIX

PROTON ACCESSIBILITY IN THE E-μ PHASE SPACE

In this appendix we recall some elementary concepts of the resolution method when dealing with protons in a nonmonotonic potential energy structure. The conservation laws (1) and (2) determine the region where the function f is defined as

$$v_{\parallel}^2 \geq 0 \Rightarrow E \geq \mu B(r) + \Psi(r). \tag{A1}$$

The relation (A1) defines the line $v_{\parallel} = 0$ for each altitude r; the distribution function f is defined only above this line, as shown in Figure 9. From now on we will call this line at the altitude r the "r limit line." Note that the slope of this line is just the amplitude of the magnetic field $B(r)$ (noted from now on as B_r). Since in our case the magnetic field is always decreasing, the sharpest limit line will be the one of the reference level r_0. Note also that the intercept of an r limit line corresponds to the total proton potential energy $\Psi(r)$ at this altitude (also noted as Ψ_r).

Let us now consider the case of a monotonic potential for the protons, i.e., a monotonically decreasing potential, which is shown in Figure 10. All limit lines (shown in Fig. 11) for all altitudes $r > r_0$ are below the r_0 limit line, and they never intersect each other (except for $\mu < 0$, which is an unphysical case). This is because both the limit line intercept and its slope are always decreasing. At a given distance r, the distribution function f is defined above the corresponding r limit line. But if the particles that are present at an altitude r are coming from the exobase r_0, their function has also to be defined at the exobase, i.e., above the r_0 limit line. In other words, the only region where the VDF is defined in the E-μ space for particles coming from (or getting back to) the exobase is above the r_0 limit line for all the altitudes. The fact that the escaping-particle region is defined by only one limit line makes the case of a monotonic potential particularly simple.

The opposite case of a monotonically increasing potential (Fig. 12) is slightly more complicated. The limit lines' slope is still decreasing, but the intercept is increasing, giving the configuration of Figure 13. Now the limit lines for the different altitudes intersect each other. If we consider two altitudes r_0 and r, with $r > r_0$ (note that r could be the maximum altitude $r_{\max}$ in the case of a nonmonotonic potential), the VDF f is defined, as before, only above the r_0 limit line and above the r limit line for the altitude r. This means that the escaping-particle region is no longer defined by only one line, but by two ones that intersect at the point (E^*, μ_r^*) with $\mu_r^* = -(\Psi_r - \Psi_0)/(B_r - B_0)$. This is the α-region shown in Figure 13. In the β-region, there are particles that are defined in r_0 but are not present in r; that is, they are ballistic and can reach altitudes up to r and then fall back to the exobase r_0.

In Figures 14 and 15, we can see the same case as before, considering the potential maximum at $r_{\max}$ and an intermediate altitude r, with $r_0 < r < r_{\max}$. If μ_r^* is the abscissa of the intersection point between the r_0 and r limit lines, we can distinguish two different cases, the first one when $\mu_r^* > \mu_{\max}^*$, i.e., the r limit line is located above the intersection point $(E^*, \mu_{\max}^*)$ (Fig. 14), and the opposite one when $\mu_r^* < \mu_{\max}^*$ (Fig. 15). In the first case, the escaping region is not defined by only two lines as in Figure 13, because these particles also have to be present at altitude r. The consequence is that a new region appears, the region ϵ, which contains ballistic particles (between r_0 and r) and not escaping ones. The totality of ballistic particles between r_0 and r are defined in region $\gamma + \epsilon$. The β-region contains ballistic particles that can reach altitudes up to $r_{\max}$. We can therefore see that the escaping-particle region α is reduced (by the ϵ-region) because of the obligatory presence of these particles in the intermediate altitude r between the exobase and $r_{\max}$.

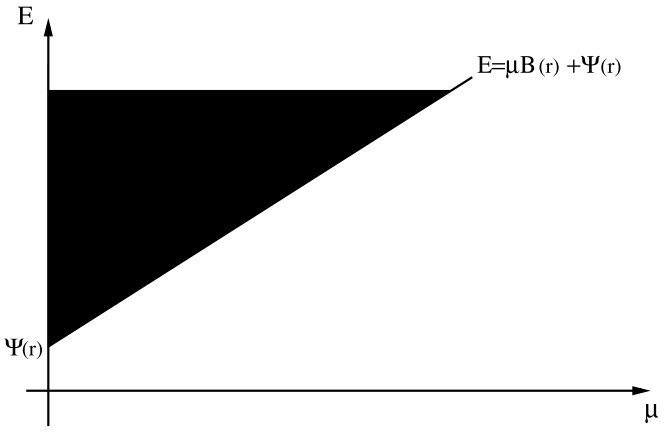

FIG. 9.—E-μ space for the altitude r. The slope of the r limit line is the amplitude of the magnetic field $B(r)$, while its intercept is the total proton potential energy $\Psi(r)$ at this altitude. The distribution function f is defined only above this limit line, i.e., in the black region.

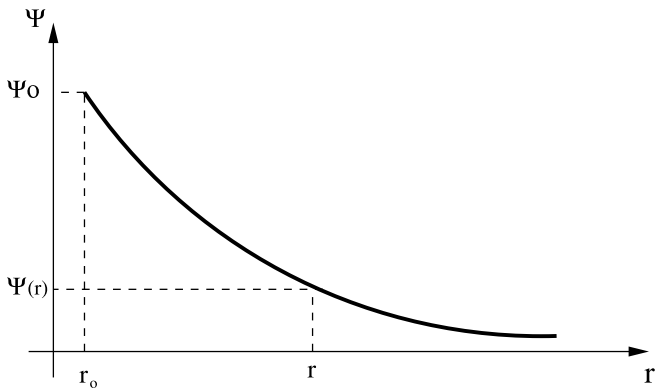

FIG. 10.—Case of an always-decreasing proton potential energy

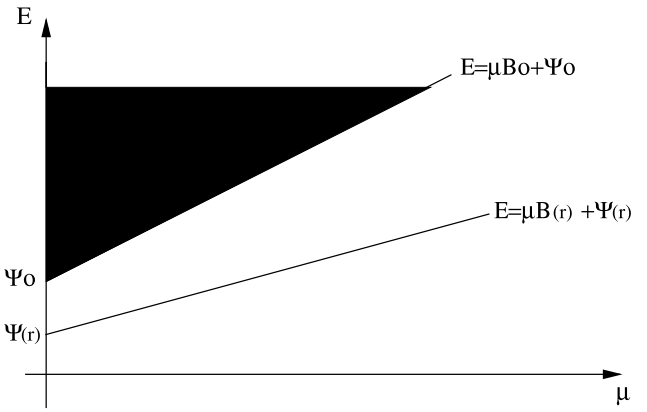

FIG. 11.—E-μ space for the decreasing potential of Fig. 10. All r limit lines are found below the r_0 one. The distribution function f is defined in the black region for all altitudes $r \geq r_0$.

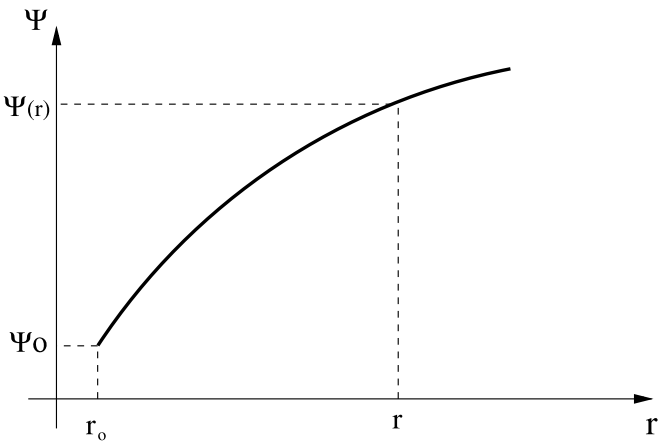

FIG. 12.—Case of an always-increasing proton potential energy

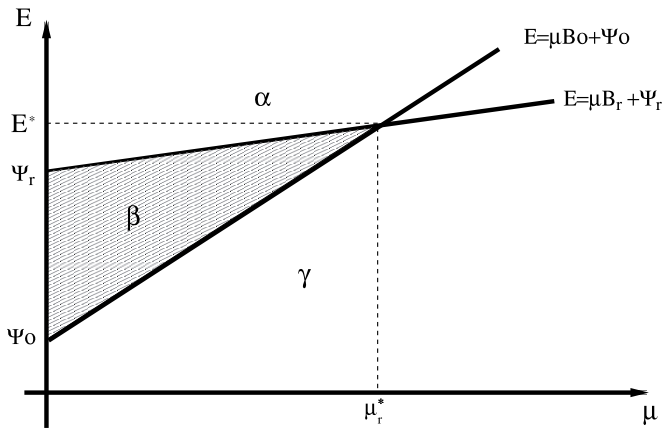

FIG. 13.—E-μ space for the increasing potential of Fig. 12. The r limit lines intersect. Protons that can escape from the altitude r are defined in the α-region. The β-region corresponds to ballistic protons, while the distribution function f is not defined in the γ-region.

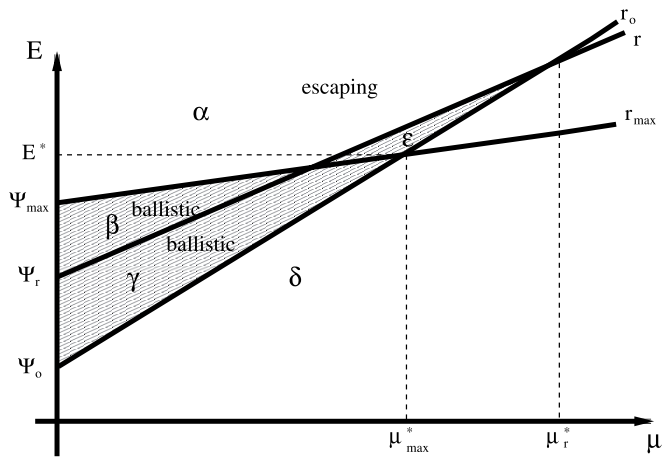

FIG. 14.—E-μ space for an increasing proton potential energy for altitudes $r_0 < r < r_{\max}$, with $\mu_r^* > \mu_{\max}^*$. The escaping-protons region α is reduced by the ϵ one, which contains ballistic protons.

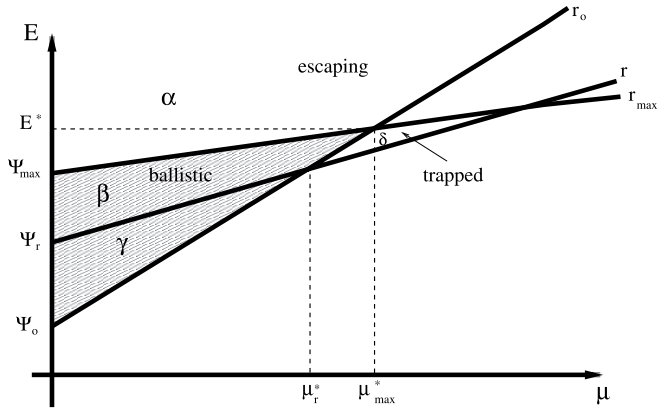

FIG. 15.—E-μ space for an increasing proton potential energy for altitudes $r_0 < r < r_{\max}$, with $\mu_r^* < \mu_{\max}^*$. The region δ corresponds to trapped particles between r and $r_{\max}$.

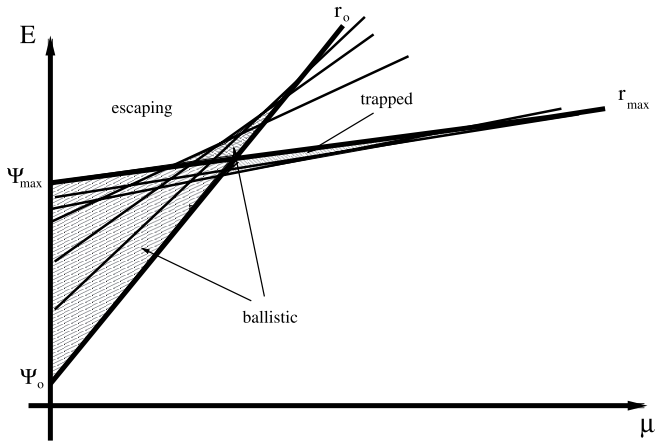

FIG. 16.—E-μ space for an increasing proton potential energy for altitudes $r_0 < r < r_{\max}$ considering the contribution of several altitudes between r_0 and $r_{\max}$

In the second case of an increasing potential (Fig. 15), the escaping region is not modified but there is now a new region (δ) with trapped particles between r and $r_{\max}$ that are defined below the r_0 limit line and therefore do not come from the exobase. It is now evident that definitions of regions of different species depend on the potential values at all intermediate altitudes between r_0 and $r_{\max}$, as shown in Figure 16. The geometrical definition of these regions is the main numerical difficulty of our problem, combined with the fact that the potential values are not known but have to be calculated a posteriori using the zero charge and current conditions.

At a given altitude r_α, we can consider an elementary region of escaping particles between two consecutive points μ_1 and μ_2 and above the r_α limit line (Fig. 17). In order to calculate a moment of the VDF in a given altitude r for the escaping particles, we have to calculate the following integral:

$$I_j(B_\alpha, \Psi_\alpha, \mu_1, \mu_2) = \int_{\mu_1}^{\mu_2} \left[\int_{E_\alpha}^{\infty} \hat{F}_j(E, \mu) dE \right] d\mu,$$

with $E_\alpha = \mu B_\alpha + \Psi_\alpha$. $\hat{F}_j$ is the appropriate kernel from definitions (3)–(6), with $B = B_r$ and $\Psi = \Psi_r$. For a bi-Maxwellian VDF, these expressions have been calculated by Khazanov et al. (1998) and will not be repeated here. All different integrals I_j then have to be added for all altitudes r_α with $\alpha = 0, \ldots, m$. This has to be done numerically.

Up to now, we have not found a general method for calculating the exact solution of the self-consistent electric potential. Therefore, we have to make an approximation on the escaping particles rate in order to find a self-consistent potential. All particles, which can be present at both r_0 and $r_{\max}$, are considered as escaping; i.e., we consider that the region labeled ϵ in Figure 14 corresponds to escaping particles at r_m, instead of ballistic particles, which do not overcome r. This important approximation is used by Jockers, with a resulting error in the particle flux claimed to be in general less than 1% (Jockers 1970). However, the errors due to this approximation may be much greater with suprathermal electrons. With this approximation there are only three unknown parameters: the position of the potential maximum $r_{\max}$ and the electric potential ϕ_{E0} at the exobase and $\phi_{E\max}$ at the maximum. The main problem is that there are only two equations (equality of fluxes at the exobase and quasi-neutrality at $r_{\max}$), but the problem has a unique solution if we suppose the existence of only one maximum, which gives the following constraints:

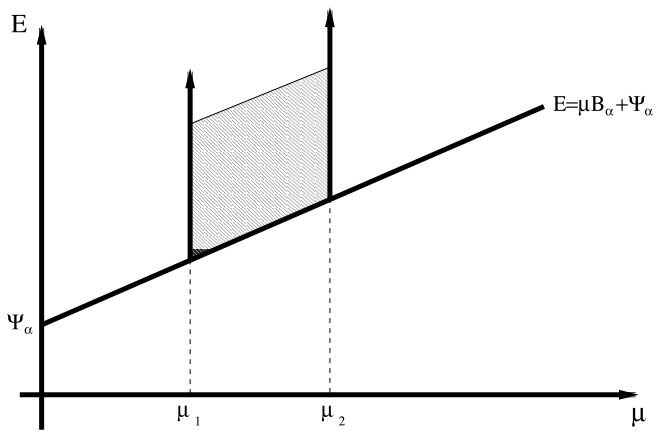

FIG. 17.—Example of an elementary region of escaping particles between two consecutive points μ_1 and μ_2 and above the r_α limit line

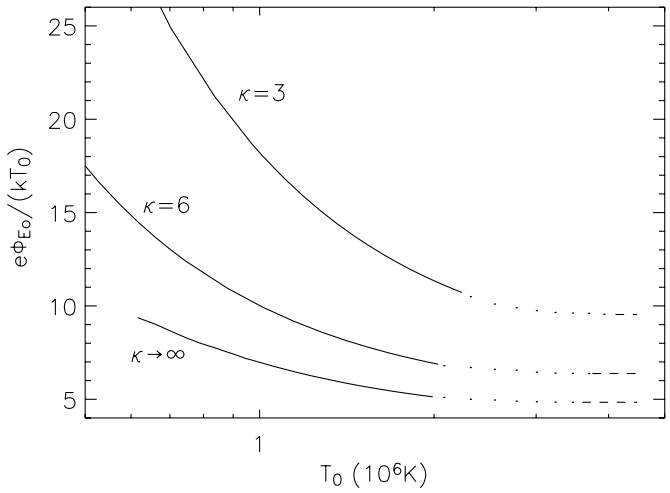

FIG. 18.—Electrostatic potential in function of the exobase temperature for different values of κ. *Solid lines*: Solutions given by the present model (nonmonotonic proton potential). *Dashed lines*: Previous exospheric models with a monotonic proton potential profile. *Dotted lines*: Range of a low numerical precision as explained in the text.

$\phi_{E\max} < \phi_{E0}$, $\Psi_{\max} > \Psi_0 \Rightarrow \phi_{E\max} > \phi_{E0} - (m_p M_\odot G/e)(1/r_0 - 1/r_{\max})$, and $\Psi_{\max} > 0 \Rightarrow \phi_{E\max} > m_p M_\odot G/(e r_{\max})$, where m_p is the proton mass. The technical details of the solution of this system can be found in Jockers (1970) and equally in Lamy et al. (2003). An important point to note is that the approach used by Lamy et al. (2003), which consists of integrating the VDF in the velocity space, leads to exactly the same results as our model, using the approximation on the ϵ-region.

In order to verify that the solutions given by the present model are consistent with those of the previous models for which the proton potential was monotonic (Maksimovic et al. 1997a), we have calculated the electrostatic potential in a range of exobase temperatures including both types of solutions. For simplicity we assume for this comparison a single kappa VDF with $T_{p0} = T_{e0} = T_0$ and take $r_0 = 5\ R_\odot$ in order to find solutions having a monotonic potential in a reasonable temperature range. In Figure 18 we see the electrostatic potential ϕ_{E0} at the exobase (normalized to $k_b T_0/e$) as a function of T_0 for different values of κ. The full lines correspond to the solutions given by the present model when the proton potential profile is not monotonic. The dashed lines correspond to the solutions obtained with a monotonic proton potential profile (Maksimovic et al. 1997a). These values are independent of the temperature and represent the lowest possible acceleration obtained by exospheric models. The dotted lines belong to the nonmonotonic regime as well, but the solutions are not known because of a low precision due to the very small difference between ϕ_{E0} and $\phi_{E\max}$. One can see that the solutions obtained in both regimes are mutually consistent, since there are no discontinuities. The approximation used on the escaping particles rate would have consequences only at the very left part of the curves in Figure 18, for which the acceleration is important and therefore the ϵ-region would become significant. For the same reasons the approximation made has more important consequences for low values of κ. In a full treatment of the problem that would not make this approximation, the calculated terminal bulk speed would be higher. This is because protons in the ϵ-region would be considered ballistic ones (instead of escaping ones) and would thus need a stronger electrostatic potential in order to escape from the gravitational well of the Sun.

REFERENCES

Brandt, J. C., & Cassinelli, J. P. 1966, Icarus, 5, 47
Chamberlain, J. W. 1960, ApJ, 131, 47
Chen, W. M., Lai, C. S., Lin, H. E., & Lin, W. C. 1972, J. Geophys. Res., 77, 1
Chen, Y., Esser, R., & Hu, Y. Q. 2003, J. Geophys. Res., 108(A10), SSH 7-1
Chiu, Y. T., & Schulz, M. 1978, J. Geophys. Res., 83, 629
Collier, M. R. 1993, Geophys. Res. Lett., 20, 1531
Cranmer, S. R. 2002, Space Sci. Rev., 101, 229
Dorelli, J. C., & Scudder, J. D. 2003, J. Geophys. Res., 108(A7), SSH 7-1
Esser, R., & Edgar, R. J. 2000, ApJ, 532, L71
Esser, R., & Sasselov, D. 1999, ApJ, 521, L145
Feldman, W. C., Asbridge, J. R., Bame, S. J., Montgomery, M. D., & Gary, S. P. 1975, J. Geophys. Res., 80, 4181
Hollweg, J. V. 1978, Rev. Geophys. Space Phys., 16, 689
Hundhausen, A. J. 1972, Coronal Expansion and Solar Wind (Berlin: Springer)
Jensen, E. 1963, Astrophysica Norvegica, 8, 99
Jockers, K. 1970, A&A, 6, 219
Khazanov, G. V., Liemohn, M. W., Krivorutsky, E. N., & Moore, T. E. 1998, J. Geophys. Res., 103, 6871
Koutchmy, S. 1977, Sol. Phys., 51, 399
Lamy, H., Pierrard, V., Maksimovic, M., & Lemaire, J. F. 2003, J. Geophys. Res., 108(A1), SSH 13-1
Landi, S., & Pantellini, F. 2001, A&A, 372, 686
———. 2003, A&A, 400, 769
Lemaire, J., & Scherer, M. 1971a, J. Geophys. Res., 76, 7479
Lemaire, J., & Scherer, M. 1971b, Phys. Fluids, 14, 1683
Leubner, M. P. 2002, Ap&SS, 282, 573
Liemohn, M. W., & Khazanov, G. V. 1998, Phys. Plasmas, 5, 580
Lin, R. P., et al. 1997, Adv. Space Res., 20, 645
Ma, C., & Summers, D. 1999, Geophys. Res. Lett., 26, 1121
Maksimovic, M., Pierrard, V., & Lemaire, J. F. 1997a, A&A, 324, 725
Maksimovic, M., Pierrard, V., & Riley, P. 1997b, Geophys. Res. Lett., 24, 1151
Meyer-Vernet, N., & Issautier, K. 1998, J. Geophys. Res., 103, 29705
Meyer-Vernet, N., Mangeney, A., Maksimovic, M., Pantellini, F., & Issautier, K. 2003, in AIP Conf. Proc. 679, Solar Wind Ten, ed. M. Velli, R. Bruno, & F. Malara (New York: AIP), 263
Neugebauer, M. 1997, J. Geophys. Res., 102, 26887
Olbert, S. 1981, in Plasma Astrophysics, ed. T. D. Guyenne & G. Levy (ESA SP-161; Paris: ESA), 135
Pannekoek, A. 1922, Bull. Astron. Inst. Netherlands, 1, 107
Parker, E. N. 1958, ApJ, 128, 664
———. 1960, ApJ, 132, 821
Pierrard, V., Issautier, K., Meyer-Vernet, N., & Lemaire, J. 2001, Geophys. Res. Lett., 28, 223
Pierrard, V., & Lemaire, J. 1996, J. Geophys. Res., 101, 7923
Pilipp, W. G., Miggenrieder, H., Montgomery, M. D., Muhlhauser, K. H., Rosenbauer, H., & Schwenn, R. 1987, J. Geophys. Res., 92, 1075
Rosseland, S. 1924, MNRAS, 84, 720
Schwartz, S. J., & Marsch, E. 1983, J. Geophys. Res., 88, 9919

Scudder, J. D. 1992, ApJ, 398, 299
———. 1996, J. Geophys. Res., 101, 11039
Shoub, E. C. 1983, ApJ, 266, 339
Treumann, R. A. 1999, Phys. Scr., 59, 19
Vasyliunas, V. M. 1968, J. Geophys. Res., 73, 2839
Viñas, A. F., Wong, H. K., & Klimas, A. J. 2000, ApJ, 528, 509
Vocks, C., & Mann, G. 2003, ApJ, 593, 1134
Zouganelis, I., Maksimovic, M., Meyer-Vernet, N., Lamy, H., & Pierrard, V. 2003, in AIP Conf. Proc. 679, Solar Wind Ten, ed. M. Velli, R. Bruno, & F. Malara (New York: AIP), 315